

## Article

# Multi-Scenario Simulation of Land Use Carbon Emissions from Energy Consumption in Shenzhen, China

Wenwen Tang <sup>1,2</sup>, Lihan Cui <sup>2</sup>, Sheng Zheng <sup>1,2,\*</sup>  and Wei Hu <sup>3,\*</sup>

<sup>1</sup> Key Laboratory of Urban Land Resources Monitoring and Simulation, Ministry of Natural Resources, Shenzhen 518034, China

<sup>2</sup> Department of Land Management, Zhejiang University, Hangzhou 310058, China

<sup>3</sup> Shenzhen Urban Planning & Land Resource Research Center, Shenzhen 518040, China

\* Correspondence: shengzheng@zju.edu.cn (S.Z.); have211@163.com (W.H.)

**Abstract:** Investigating the future land use patterns and carbon emissions are of great significance for carbon reduction. This study established the relationship between land use types and carbon emissions from energy consumption and adopted three future scenarios that combine shared socioeconomic pathways (SSPs) and representative concentration pathways (RCPs), the system dynamics (SD) model, and the patch-generating land use simulation (PLUS) model to simulate land use patterns in 2030 and 2035. Then the spatial distribution of future carbon density and its change in Shenzhen were obtained. Under scenario SSP245, a large amount of industrial and mining land is converted into living land from 2020 to 2035, and new living land is mainly located in Bao'an District and Guangming District. Under scenario SSP370, a large amount of living land replaces other land due to a plentiful population from 2020 to 2035, which is rare under other scenarios. The expansions of areas with high carbon density during 2020–2030 are mainly distributed in Nanshan District and Longhua District under all three scenarios. During 2030–2035, carbon emissions will decrease under scenarios SSP126 and SSP245. The results confirmed various trends in carbon emissions under different scenarios and emphasized the association between land use types and carbon emissions.



**Citation:** Tang, W.; Cui, L.; Zheng, S.; Hu, W. Multi-Scenario Simulation of Land Use Carbon Emissions from Energy Consumption in Shenzhen, China. *Land* **2022**, *11*, 1673. <https://doi.org/10.3390/land11101673>

Academic Editor: Nir Krakauer

Received: 23 August 2022

Accepted: 23 September 2022

Published: 28 September 2022

**Publisher's Note:** MDPI stays neutral with regard to jurisdictional claims in published maps and institutional affiliations.



**Copyright:** © 2022 by the authors. Licensee MDPI, Basel, Switzerland. This article is an open access article distributed under the terms and conditions of the Creative Commons Attribution (CC BY) license (<https://creativecommons.org/licenses/by/4.0/>).

**Keywords:** land use patterns; carbon density; PLUS model; shared socioeconomic pathways

## 1. Introduction

Land use patterns on Earth are closely related to anthropogenic exploitation and natural processes. The carrier of human activities and terrestrial ecosystem cycles is land, and frequent changes in land use have an impact on carbon emissions [1,2]. Carbon emissions from fossil energy combustion are mainly accounted for anthropogenic activities and these activities are always based on built-up land [3], including urban residential land, traffic land, and industrial land. Thus, carbon emissions vary considerably depending on the type of land use [4], and the expansion of land associated with a high carbon emission density might lead to increases in total carbon emissions. A rational land use pattern is conducive to low-carbon development and the achievement of China's pledged goal of carbon peak and carbon neutrality at the General Debate of the 75th Session of the United Nations General Assembly [5]. In addition, the 2035 Vision targets propose that China will complete basic socialist modernization in 2035, with a steady decline in carbon emissions after reaching a peak [6]. To achieve these goals, accurate projections of the trends in land use carbon emissions in 2030 and 2035 are necessary to support the formation of future land-use regulation policy.

Scholars have made some attempts to account for land use carbon emissions. Zhao and Huang [7] matched the land use types with carbon emission items to explore the carbon emissions from energy consumption of different land use types in Jiangsu Province. Zhao et al. [8] discussed the carbon emission intensity of different industrial spaces in China and found that living and industrial-commercial space, as well as transportation industrial

space, were industrial spaces with high carbon emissions. Wu et al. [9] established the relationship between different types of land and carbon emissions in Zhejiang Province and concluded that carbon emissions were driven by the inelastic demands of energy-intensive land. Due to technological innovation, some cities, such as Shenzhen, have achieved widespread adoption of electric vehicles [10,11], which has a certain impact on the carbon emissions of road transportation [12]. As a result, the previous conclusions about land use carbon emissions should be challenged and updated. Previous research [7–9] adopted the term “carbon intensity” to represent carbon emissions per unit of land area, while “carbon intensity” is more frequently used to refer to “carbon emissions per unit of gross domestic product (GDP)” [13–17]. To avoid any ambiguities, energy-related CO<sub>2</sub> emissions per unit of land area in this study is represented by “carbon density” instead of “carbon intensity”.

Simulation and prediction of future situations require setting various scenario assumptions and analyzing potential changes under different paths. Existing studies generally designed a baseline scenario and several comparison scenarios by controlling for change rates of parameters [18–20]. However, these specific indicators and scenario designs depend on the researchers’ subjective judgments about the future. In addition, climate change has an impact on land use that cannot be ignored [21,22], which was less often considered in land use scenario design. O’Neill et al. [23] proposed five shared economic pathways (SSPs) from two dimensions of socioeconomic challenges faced by humans in mitigating and adapting to climate change, respectively. Domestic scholars have applied SSPs to predict precipitation [24,25], temperature [25,26], population [27], urban land expansion [28], land use dynamics [29], and land use demand [30]. Shared socioeconomic pathways (SSPs) were combined with representative concentration pathways (RCPs) in Phase 6 of the Coupled Model Intercomparison Project (CMIP6) to define more reasonable future scenarios under the background of global climate change [31–33]. SSP-RCP scenarios have been adopted by an increasing number of scholars to simulate land use changes in the future. Dong et al. [34] designed eight scenarios with various combinations of SSPs and RCPs to predict future land use demand and discovered that the future land patterns varied greatly depending on the scenario. Wang et al. [35] simulated future land use/cover change (LUCC) in Bortala using projected socioeconomic and climate data from existing studies under three SSP-RCP scenarios. They analyzed the distribution of different land use types, including cultivated land, pasture areas, grassland, and construction land, without discussing the situation of various construction land. SSP-RCP scenarios are adopted in this study to incorporate climate change into land use patterns simulations in Shenzhen, and construction land is split into various categories, further filling the gap in existing studies.

In the field of simulating the spatial distribution of different types of land, studies have been conducted to develop simulation models with increasing accuracy. The cellular automata (CA) model is a dynamic model that focuses on spatiotemporal interactions and underlying rules, which is well suited to simulating intricate geographic evolution processes [36]. Many simulation models based on CA models have been widely used in land use studies, including Logistic-CA [37,38], CA-Markov [39,40], ANN-CA [41], and FLUS model [28,34,42]. These models, which can produce valuable results, are either based on the transition analysis strategy (TAS) or based on the pattern analysis strategy (PAS). However, they can neither adequately disclose the driving factors of land use types transitions and their contributions to land change [43], nor can they simulate multiple land use types at the patch level with spatiotemporal dynamics [35]. An improved patch-generating land use simulation (PLUS) model combines the advantages of TAS and PAS but overcomes their weaknesses through a random forest classification (RFC) algorithm [36,44], while satisfying the requirement for patch-level simulation of multiple land use types based on random seed growth mechanisms [20], which increases accuracy. Although some scholars have adopted the PLUS model in their studies and obtained high simulation accuracy [20,30,36,44,45], the PLUS model has not yet been applied as a new method to simulate multiple types of land use changes in Shenzhen, a developed city with complex land use patterns [46].

Land use changes in Shenzhen, Guangdong Province, have intensified [47] and become more diverse due to location and regional industrial development [48]. This study took Shenzhen City as the study area and firstly constructed the relationship between land use types and carbon density, i.e., energy-related CO<sub>2</sub> emissions per unit of land area, and predicted land use demand under three SSP-RCP scenarios based on a system dynamic (SD) model. The land use patterns in 2030 and 2035 were simulated using the PLUS model. The distribution of future land use carbon density in Shenzhen was obtained, and its spatial variations were analyzed to put forward some valuable policy recommendations. The purposes of this study were to (1) predict land use demand precisely using the SD model and SSP-RCP scenarios, taking into account future climate change; (2) obtain more accurate future land use patterns using the PLUS model; and (3) associate land use types with carbon emissions and analyze carbon density change in the future. The greatest novelty of this study is the fact that climate change is included in the land use patterns simulations, with construction land split into different types such as industrial and mining land, traffic land, etc., and their possible future distributions are discussed separately, providing a new perspective to simulate future land use patterns.

## 2. Materials and Methods

In this study, the relationship between land use types and carbon emissions was constructed. Meanwhile, land use demand under future scenarios was predicted using SSP-RCP scenarios and the SD model. Then, land use data in 2015 and 2020 and various driving factors were adopted to validate the PLUS model, followed by the simulation of land use patterns in 2030 and 2035 with the constraint of predicted future land use demand. Finally, spatiotemporal variations of land use carbon density in Shenzhen were discussed incorporating the relationship between land use types and carbon emissions and simulated results of future land use patterns. In summary, the technical flowchart of this study is shown in Figure 1.

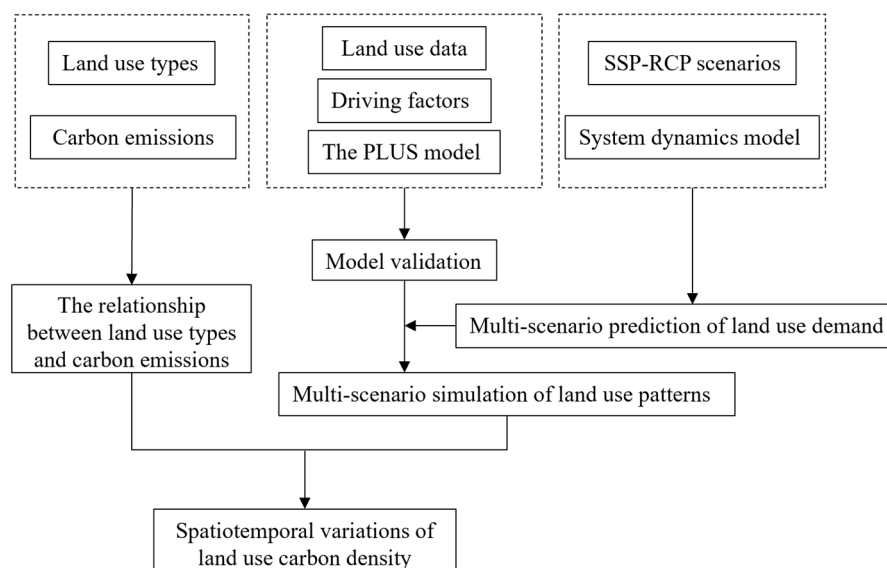


**Figure 1.** Technical flowchart.

### 2.1. Study Area and Data Sources

Shenzhen is located on the eastern bank of Pearl River Estuary in the southern coastal area of Guangdong Province. As shown in Figure 2, Shenzhen ranges geographically between 113°43' E–114°38' E and 22°24' N–22°52' N, occupying an area of 1986 km<sup>2</sup> in 2020. It is a megacity with a total population of 17.63 million in 2020 and a population density of 8879 person/km<sup>2</sup>, which explains its scarcity of land resources. It is composed of 9 administrative districts, including Bao'an District, Guangming District, Nanshan District,

Futian District, Luohu District, Longhua District, Yantian District, Pingshan District, and Longgang District.

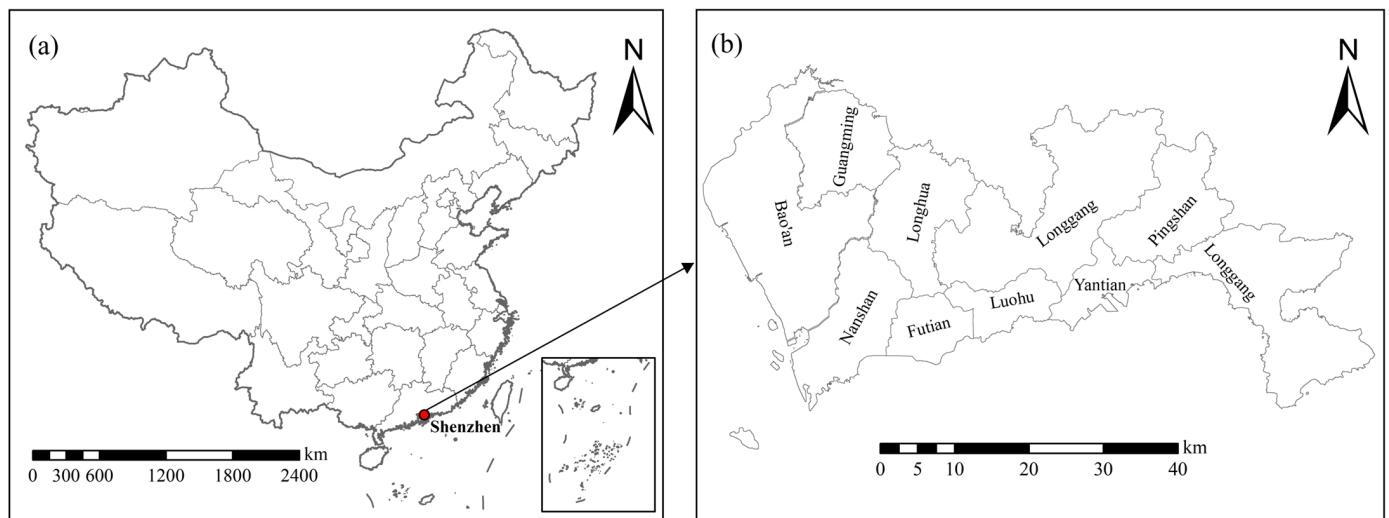


**Figure 2.** (a) Location of Shenzhen in China; (b) the administrative districts in Shenzhen.

Energy consumption data and its composition were referred to Shenzhen Statistical Yearbook (2015–2020) and Shenzhen 13th Five-Year Plan for Energy Development (2015–2020). The SD model required figures of GDP, population, annual average temperature, annual average precipitation, investment in fixed assets, and growth rate of investment in fixed assets of each national economic industry. These figures were obtained from Shenzhen Statistical Yearbook (2015–2020). Data required in the PLUS model should be in raster form, different from data adopted in the SD model. Population data were extracted from Population Count datasets of WorldPop (<https://hub.worldpop.org>, accessed on 17 March 2022). Land use data of Shenzhen from 2015 to 2020 was obtained from the Land Use Change Survey data of the Shenzhen Municipal Bureau of Planning and Natural Resources. The five land categories of industrial and mining land, traffic land, living land, agricultural land and water area, and other land were obtained through land category consolidation and then rasterized to 30 m resolution. GDP, temperature, and precipitation were obtained from the Data Center for Resources and Environmental Sciences of the Chinese Academy of Sciences [49,50]. Nighttime light data were extracted from the VIIRS\_DNB\_VNL V2 datasets of the Earth Observation Group (EOG) [51]. Digital elevation model (DEM) data were obtained from NASADEM\_HGT V001 datasets [52], from which slope and degree of relief were calculated. Vector data such as cities, towns, waters, rivers, railways, motorways, and other roads from OpenStreetMap (<https://www.openstreetmap.org>, accessed on 18 February 2022) were adopted and processed into raster data by Euclidean distance analysis. Data for all driving factors used are from 2015.

## 2.2. Energy-Related Land Use Carbon Density

As a carrier of various natural processes and human activities, different uses inevitably affect the carbon density on the land [4]. This study adopted the method of Zhao and Huang [7] and divided different land use types into five categories (Table 1): industrial and mining land, traffic land, living land, agricultural land and water area, and other land. To assign carbon emissions to each type of land, energy consumption of several sectors was merged. Carbon emissions on industrial land and mining land stem from the energy consumption of industry. Energy consumptions of transportation, storage, postal and telecommunication services contribute to traffic land use carbon emissions. Living land in this study carries human activities such as eating, trading, entertaining, receiving medical treatment, and schooling. Therefore, living land use carbon emissions derive

from energy consumption of residential lifestyles, wholesale and retail trade and catering, construction, and services others. Carbon emissions on agricultural land and water area derive from energy consumption of farming, forestry, animal husbandry, and fishery. Other land includes special designated land and unused land. Some scholars assigned energy consumption of “other industries” to other land [8,53] or neglected directly [3]. However, there is only an energy consumption item called “services others” which represents other service industries in the tertiary sector in Shenzhen Statistical Yearbook, and its figures are not negligible. Therefore, this study allocated the energy consumption of services others to living land, similar to the approach taken by Wu et al. [9]. As a matter of course, it was assumed that human activities that generate carbon emissions do not take place on other land. Energy-related carbon emissions were calculated based on the IPCC method [54]:

$$CE_k = \sum SC \times E_i \times \alpha_i \times 44/12 \quad (1)$$

where  $CE_k$  ( $10^4$  tons) refers to the energy-related  $CO_2$  emissions of each land use type,  $k = 1, 2, 3, 4, 5$ ;  $SC$  represents the consumption of standard coal;  $E_i$  depicts the proportion of energy consumption of  $i$ th fossil fuel energy; and  $\alpha_i$  means the emission factor of the  $i$ th fossil fuel energy. The fossil fuel energy in this study consists of coal, oil and natural gas. The emission factors are taken from the research results of the Energy Research Institute of the National Development and Reform Commission, where the carbon emission factors for coal, oil, and natural gas are 0.7476 t/tce, 0.5825 t/tce, and 0.4435 t/tce, respectively.

**Table 1.** Relationship between land use types and energy-related carbon emission items.

Land Use Types	Specific Types	Energy Consumption/Carbon Emission Items
Industrial and mining land	Industrial land Mining sites	Industry
Traffic land	Transportation land Warehousing land	Transportation, storage, postal, and telecommunication services
Living land	Urban residential land Rural residential land Commercial land Public administration and public service sites	Residential consumption Construction Wholesale and retail trade and catering Services others
Agricultural land and water area	Cropland Garden area Woodland Grassland Water and Water Facilities Land	Farming, forestry, animal husbandry, and fishery
Other land	Special designated land Unused land	None

Energy-related land use carbon density can be represented by  $CO_2$  emissions per unit of land area and obtained by the following formula:

$$CI_k = \frac{CE_k}{S_k} \quad (2)$$

where  $CI_k$  (t/ha) refers to the energy-related carbon density of land use type  $k$ , and  $S_k$  ( $m^2$ ) represents the total area of land use type  $k$ . The carbon density on each type of land use in 2030 and 2035 were set using the mean value of carbon density on each land use type during 2015–2020.

### 2.3. Land Use Demand Prediction Using Future Scenarios and System Dynamics Model

The Scenario Model Intercomparison Project (ScenarioMIP) is the major project of CMIP6, consisting of eight future pathways. These eight pathways are divided into two tiers, and tier 1 contains a wide range of uncertainties in future forcing pathways and key scenarios, including SSP126, SSP245, SSP370, and SSP585 [55]. SSP126 incorporates SSP1

and RCP2.6, representing a sustainable socioeconomic development pathway with a low radiation forcing which peaks at  $2.6 \text{ W/m}^2$  by 2100. SSP245 is the combination of SSP2 and RCP4.5, which represents a moderate socioeconomic development path that continues historical patterns with medium-low radiation forcing which peaks at  $4.5 \text{ W/m}^2$  by 2100. SSP370 combines the SSP3 with RCP7.0, representing a medium-high socioeconomic development path with radiation forcing which peaks at  $7.0 \text{ W/m}^2$  by 2100. SSP585 represents a highly energy-intensive scenario and the number of its emissions is high enough to bring the radiation forcing to  $8.5 \text{ W/m}^2$  by 2100 [35,56,57]. Both SSP126 and SSP 585 are positive human development pathways, and the difference is that SSP126 is a sustainable practice, while SSP585 has an energy-intensive economy [55]. However, Shenzhen has achieved a strong decoupling of economic growth and carbon emissions [58,59], which means economic growth in Shenzhen no longer comes at the cost of increased carbon emissions [60]. Thus, the scenario with the most rapid economic development based on high energy consumption is not in line with the reality in Shenzhen and is not considered in this study. Future scenarios were decided by four parameters: population, GDP, annual average temperature, and precipitation. The future data for Shenzhen was extracted from existing predicted data and change rates were calculated to obtain the values of parameters after 2020. The values of socioeconomic factors were calculated using future predicted grid data of population [27] and GDP [61] under SSPs scenarios. The future climate data were obtained based on the model output of the medium-resolution Beijing Climate Center Climate System Model version 2 (BCC-CSM2-MR) [62].

The system dynamics (SD) model is an effective tool to allow the evolution of a complex system to be predicted through the feedback and interactions among various elements [63]. This study assumed that land use demand can be only determined by GDP, population and climate change (temperature and precipitation) in the SD model. GDP is linked with investment in fixed assets. Investment in each type of land is the investment in corresponding national economic sectors carried on it. Population increases can contribute to the expansion of living land and traffic land due to greater demand for houses and roads. More population can also bring increasing demand for agricultural products and livestock products, but Shenzhen is a food inflow city, so this effect is negligible. Climate change mainly affects agricultural land and water area through temperature and precipitation. Based on the socioeconomic data, climate data, and land data from 2015 to 2020, the SD model of land use demand in Figure 3 was constructed, and the quantitative relationships between variables were analyzed and finally determined through several experiments. The future land use demand under each SSP-RCP scenario was simulated according to this SD model.

#### 2.4. Patch-Generating Land Use Simulation (PLUS) Model

The PLUS model derives from the CA model and integrates the dynamics of geographical cells with the impacts of various factors over space to enhance prediction ability [36]. It involves two main modules, i.e., a rule mining module based on a land expansion analysis strategy (LEAS) and a CA module based on multi-type random seeds (CARS). The LEAS excavates the impacts of various driving factors on land expansion using the random forest classification algorithm and derives the spatial distribution of development potential for each type of land. The LEAS calls for the input of land data for two dates and then extracts cells with a change in state from the later dated land data. To procure transition rules, the training dataset is used to train the data mining algorithm [43]. The CARS includes a patch-generation mechanism and simulates local land competition to adjust the amount of land to meet future demands through development potential, self-adaptive coefficient, and neighborhood effect [35]. The development potential derives from the result of the LEAS module. The self-adaptive coefficient of cells is determined by the gap between the number of existing cells in their own types and their future demands, and the neighborhood effect of a land use cell is influenced by the proportion of cells in its type and the priori diffusion coefficient [36].

Land use data for 2015 and 2020 was input to the LEAS module, and waters were extracted as the conversion constraint area. The neighborhood weight represents the expansion ability of each land-use type [30]. In this study, the neighborhood weight of each type of land use shown in Table A1 was determined by calculating the proportion of the expansion areas of a land-use type to the total land expansion based on the land expansion map (the map outputted in the LEAS module). A total of 14 driving factors of the land use change were selected and listed in Table A2, including population, GDP, the distance from town, the distance from highway, the distance from railway, the distance from other roads, nighttime light index, annual mean temperature, annual precipitation, DEM, slope, degree of relief, the distance from waters, and the distance from waterways. Taking land use data in 2015 as the initial land use pattern and applying the PLUS model, the simulation results of the land use pattern in 2020 were finally obtained. Comparing the simulated land use pattern and the actual land use pattern in 2020, the simulation accuracy can be evaluated by the Figure of Merit (FoM) metric, the kappa coefficient, and the overall accuracy. The FoM can reflect consistency at the unit level and similarity at the pattern level, with a value mostly falling between 0 and 0.3 [44]. The kappa coefficient proposed by Cohen [64] is commonly used to verify the consistency between two data images [45] and has values ranging from  $-1$  to  $1$ , with higher values representing better consistency [20]. The predicted land use demand in 2030 and 2035 under future scenarios were input into the CARS module of the validated PLUS model to simulate future land use patterns.

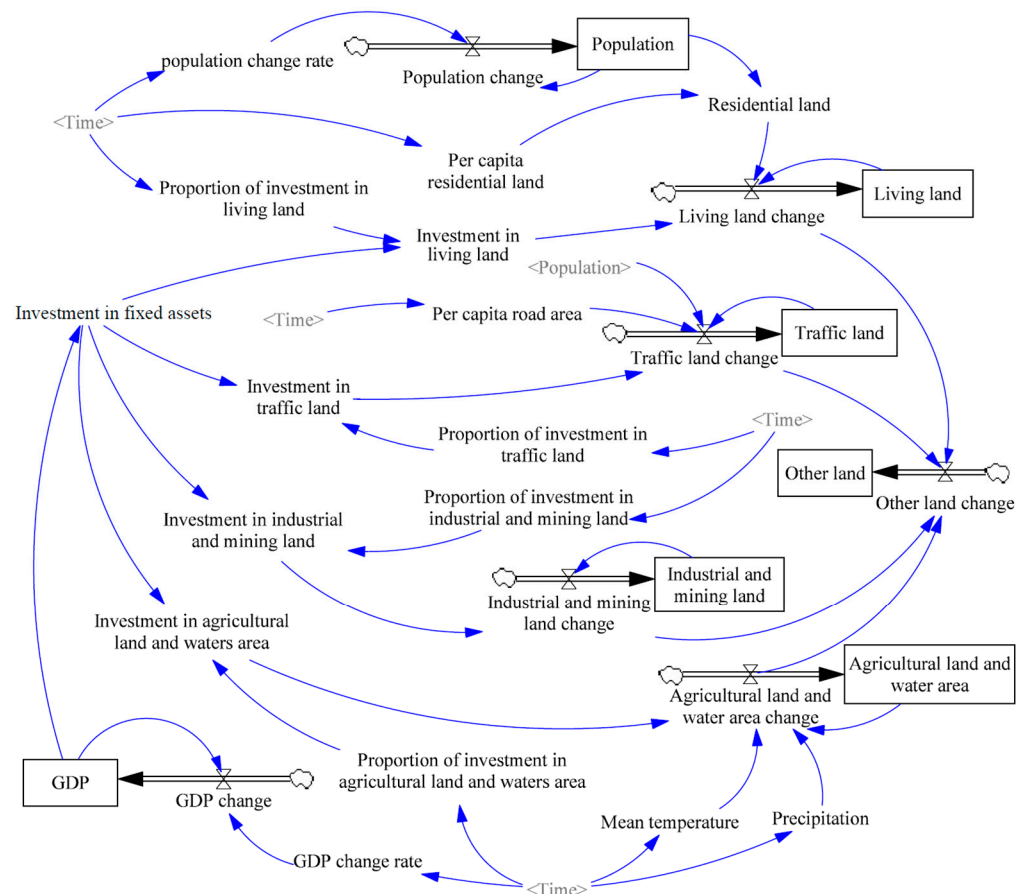


Figure 3. The system dynamics (SD) model of land use demand in Shenzhen.

### 3. Results and Discussion

#### 3.1. Energy-Related Land Use Carbon Density

According to the relationship between land use types and carbon emission items defined above, energy-related carbon density on each type of land in Shenzhen during 2015–2020 is displayed in Table 2. The total energy-related land use carbon emis-

sions in Shenzhen increased from 40.63 million tons in 2015 to 46.00 million tons in 2020, while carbon density increased from 203.45 t/ha in 2015 to 231.60 t/ha in 2020. Ke et al. [65] calculated total carbon emissions in Shenzhen and found that the amount of carbon emissions in 2015 is 13.68 MtC (million metric tons of carbon), which is close to the result of 11.08 MtC (12/44 of 40.64 million tons of CO<sub>2</sub>) in 2015 in this study. The mean carbon density is in the following order from highest to lowest: industrial and mining land > living land > traffic land > agricultural land and water area. Industrial and mining land use carbon density kept decreasing until 2019, while the carbon density on traffic land changed oppositely. Shenzhen actively promoted the transformation of inefficient industrial land into emerging industry in recent years [48], which improved the intensive use of industrial land but concentrated industrial activities on fewer amounts of land, resulting in a higher carbon density of industrial and mining land. The intensive industrial land use had been proved to be conducive to carbon reduction [66], and efficient utilization of energy through improved technology will be an effective way to control carbon density in the future. The carbon density on traffic land began to decrease in 2019, which can be attributed to the widespread adoption of electric buses [10–12]. If electric private cars also become common in the future, the carbon reduction situation will be more optimistic. Living land is home to a large population, which explains its high carbon density between 436.02 t/ha and 551.41 t/ha. Carbon density on agricultural land and water area fluctuated between 0.90 t/ha and 1.70 t/ha, much less than carbon density on other types of land.

**Table 2.** Carbon density (t/ha) on different types of land during 2015–2020.

Land Use Types	2015	2016	2017	2018	2019	2020	Mean Value
Industrial and mining land	610.58	591.77	587.52	558.93	779.91	720.68	641.56
Traffic land	294.76	321.45	345.18	372.65	363.08	312.09	334.87
Living land	470.24	488.83	517.97	551.41	436.02	462.15	487.77
Agricultural land and water area	1.13	1.67	0.90	1.36	1.70	1.19	1.33
All lands	203.45	217.46	226.82	234.08	243.48	231.60	226.15

### 3.2. Predicted Land Use Demand under Multiple Scenarios

The simulated values of various land use types in 2020 and their actual values were compared to test the simulation accuracy of the SD model. According to the results shown in Table 3, relative errors are all less than 5%, indicating that the SD model constructed can be considered to have a high simulation accuracy [35]. Using this SD model, future demand for each type of land use under three SSP-RCP scenarios were predicted and displayed in Figure 3. The trajectories of demand in Figure 4 indicates that different types of land have distinct changes, and these changes vary considerably under different SSP-RCP scenarios. The demand for industrial and mining land decreases under all scenarios. In contrast, the demand for living land keeps growing under all three scenarios, with a maximum growth rate of 13.3% under scenario SSP370. The demand for traffic land increases under all scenarios before 2030, then this demand increases only marginally during 2030–2035, and even turns to drop under scenario SSP126. Due to volatile climate, the demand for agricultural land and water area varies greatly at different times and, of course, under different scenarios. The scenario SSP370 has the most dramatic decline in the demand for agricultural land and water area. Under scenario SSP126, a sustainable socioeconomic development scenario, changes in the demand for agricultural land and water area are relatively stable. As the total amount of land in Shenzhen is considered to be unchanged, the land outside the area of the four land types mentioned above is counted as other land. The area of other land (unused land and special designated land) is largest under scenario SSP126 and smallest under scenario SSP370.

**Table 3.** The accuracy test of system dynamics (SD) model simulation results.

Land Use Types	Simulated Value in 2020 (ha)	Actual Value in 2020 (ha)	Relative Error (%)
Industrial and mining land	22569.4	22508.7	0.27%
Traffic land	27197.6	27352.2	−0.57%
Living land	46206.7	45693.0	1.12%
Agricultural land and water area	100437.0	100953.9	−0.51%
Other land	2187.1	2090.6	4.61%

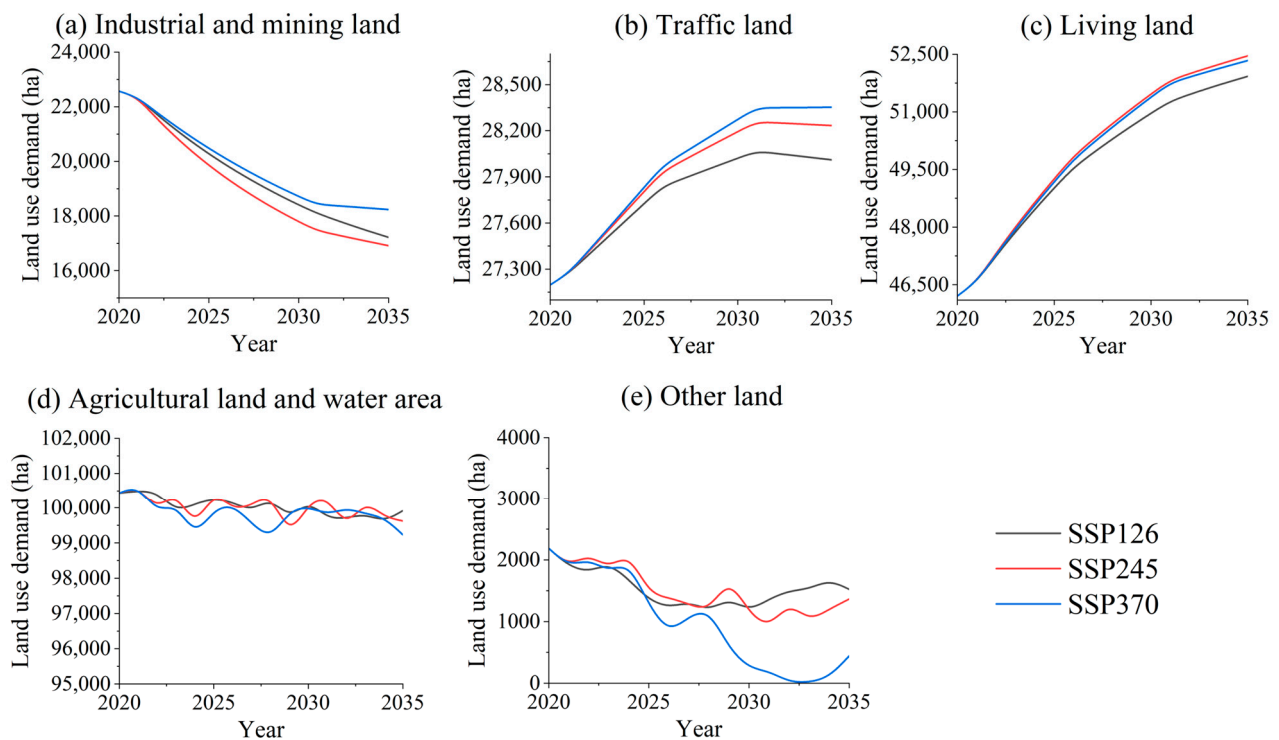


**Figure 4.** Trajectories of demand for each land use type from 2020 to 2035 under SSP-RCP scenarios: (a) future demand for industrial and mining land; (b) future demand for traffic land; (c) future demand for living land; (d) future demand for agricultural land and water area; (e) future demand for other land. Note: SSP is the abbreviation for shared socioeconomic pathways and RCP is the abbreviation for representative concentration pathways.

### 3.3. Simulated Land Use Patterns under Multiple Scenarios

The results of the PLUS model validation show a kappa coefficient of 0.69, an overall accuracy of 0.79, and a FoM of 0.09, indicating that simulation results have substantial consistency with the actual land use patterns [30,44]. Therefore, the PLUS model can accurately reflect historical variations in the land use pattern and simulate future changes in Shenzhen. The future land use patterns under SSP-RCP scenarios generated by the CARS module of the PLUS model were shown in Figure 5. Compared to other scenarios, the conversion of industrial and mining land to living land during 2020–2035 is the largest under scenario SSP245, followed by the scenario SSP126. Most of the new living lands are located in Bao’an District and Guangming District. As new special economic zones with convertible land still available, the industrial-dominated high-tech industrial zones in Bao’an Districts and Guangming District have gradually evolved into comprehensive urban areas, which can attract residents to settle down and drive the emergence of new living land in these areas [67]. A considerable amount of living land expands at the expense of other land during 2020–2035, especially under scenario 370, but this phenomenon is rare under scenarios SSP126 and SSP245. The total population is highest under scenario SSP370, which drives other land to convert into living land. Most of the emerging traffic

land during 2020–2035 originates from industrial and mining land and agricultural land and water area and is distributed along the original traffic land.

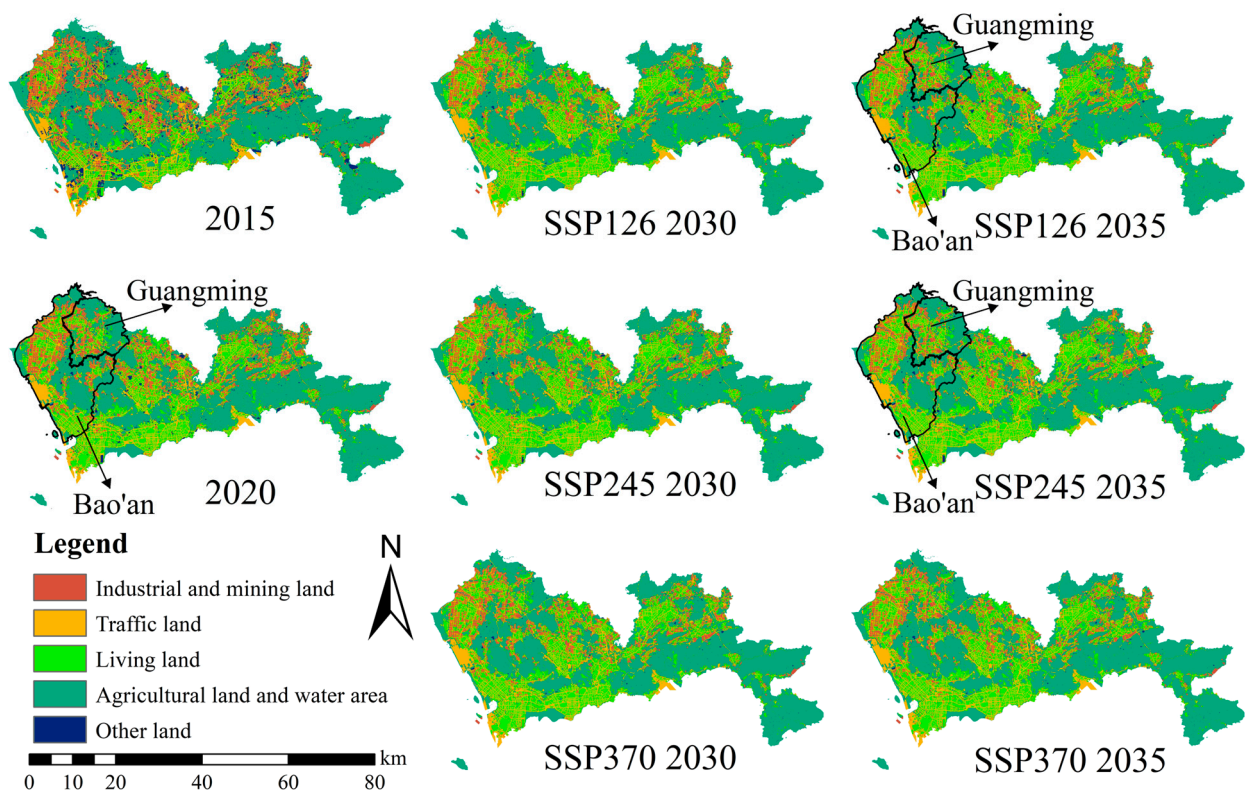


**Figure 5.** Future land use patterns under SSP-RCP scenarios in Shenzhen.

### 3.4. Spatiotemporal Variation of Land Use Carbon Density in 2015, 2020, 2030, and 2035

Using the relationship between land use types and carbon density constructed above (Table 2) and future land use patterns (Figure 4), the total carbon emissions and spatial distribution of future land use carbon density in Shenzhen can be obtained. The results of total carbon emissions illustrated the different trends under three SSP-RCP scenarios. The total amount of carbon emissions in 2020 was 46.00 million tons, an increase of 13.2% compared to that in 2015. Under scenarios SSP126, SSP245, and SSP370, total carbon emissions continuously grow after 2020. The amount of carbon emissions in 2030 under SSP370 is the largest, reaching 46.26 million tons, and it still increases to 46.56 million tons in 2035. However, the amount of carbon emissions in 2035 under SSP126 and SSP245 shows a decline compared to 2030, and this decline is more pronounced under SSP126. The total carbon emissions in 2035 under scenarios SSP126 and SSP245 is 45.79 million tons and 45.93 million tons respectively. Compared to the emissions in 2030, Shenzhen's total land use carbon emissions in 2035 will only decrease under scenarios SSP126 and SSP245, indicating that the achievement of carbon peak is possible under these two scenarios.

Figure 6 depicts the spatial distribution of land use carbon density in 2015, 2020, 2030, and 2035 under multiple scenarios. High carbon density areas are mostly distributed in the northern regions of Shenzhen, including Bao'an District, Guangming District, Longhua District, Longgang District, and Pingshan District. Compared with 2015, there was a significant decline in the amount of high carbon density areas in Longhua District and Nanshan District in 2020. To more specifically analyze future changes in land use carbon density, the changes in carbon density in 2030 compared to carbon density in 2020 and the changes in carbon density in 2035 compared to carbon density in 2030 are spatially distributed as shown in Figure 7. Under scenarios SSP126 and SSP245, the expansions of high carbon density areas in 2030 are mainly distributed in Longhua District, Nanshan District, Futian District, and Luohu District. However, these extended areas return to

low carbon density areas in 2035, and this change is more obvious under scenario SSP126. Compared with the changes under the previous two scenarios, the emerging high carbon density areas in 2030 under scenario SSP370 are concentrated in Longhua District, Yantian District, Nanshan District, and Longgang District. The scenario SSP370 still shows a few concentrated expansions of high carbon density areas in 2035, mainly in Bao'an District and Longgang District. High carbon density areas in Nanshan District and Longhua District exhibit a significant expansion under all three scenarios SSP126, SSP245, and SSP370. Both districts are located in the western part of Shenzhen, with rapid urban development and high population density [68], which can stimulate the growth of carbon emissions [69,70].

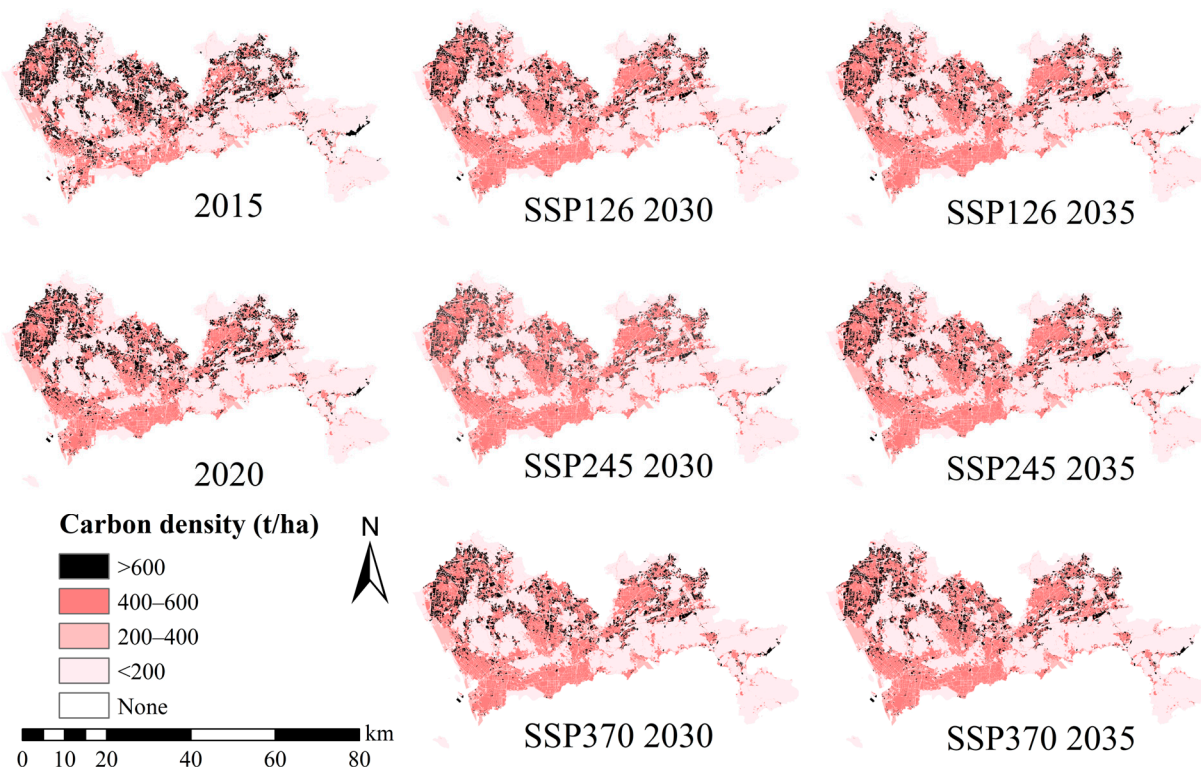


**Figure 6.** The distribution of land use carbon density under SSP-RCP scenarios in Shenzhen.

### 3.5. Uncertainties

While predictions can provide valid information for Shenzhen, there exist some uncertainties as well. The carbon emissions on one land use type are assumed to be homogeneous due to limited statistics, which is not the case in reality. For example, both residential land and public service sites are classified as living land, but these two types of land might not have the same carbon density, let alone the difference in energy consumption between light and heavy industry. Moreover, carbon density on each land use type is assumed to be a constant after 2020, which limits the results of this study for that carbon density changed obviously during 2015–2020. In the future, the prediction of energy consumption under different scenarios can be a topic of interest. In addition, the scale of the traffic land data is too fine, which might result in a simulation inaccuracy of traffic land in the PLUS model. In practice, changes in traffic land often arise from organized transport planning and are mostly in the form of a whole road, which cannot be predicted accurately through several socioeconomic and natural influencing factors. Last but not least, the scale effect can be further investigated. When choosing data in this paper, data at a finer resolution was preferred, and several simulations of land use patterns in 2020 were performed using data from different sources and validated by the kappa coefficient to generate a comparison, through which the best series of data sources that would lead to higher accuracy were identified. However, the future data under SSP-RCP scenarios adopted in the SD model

were extracted from global scale raster datasets and might not be sufficiently accurate at the city level, which is inevitable in the absence of data. More studies on SSP-RCP scenarios for China, and even for specific provinces and cities, are expected in the future to provide the basis for various investigations of the future human living environment under the background of climate change.

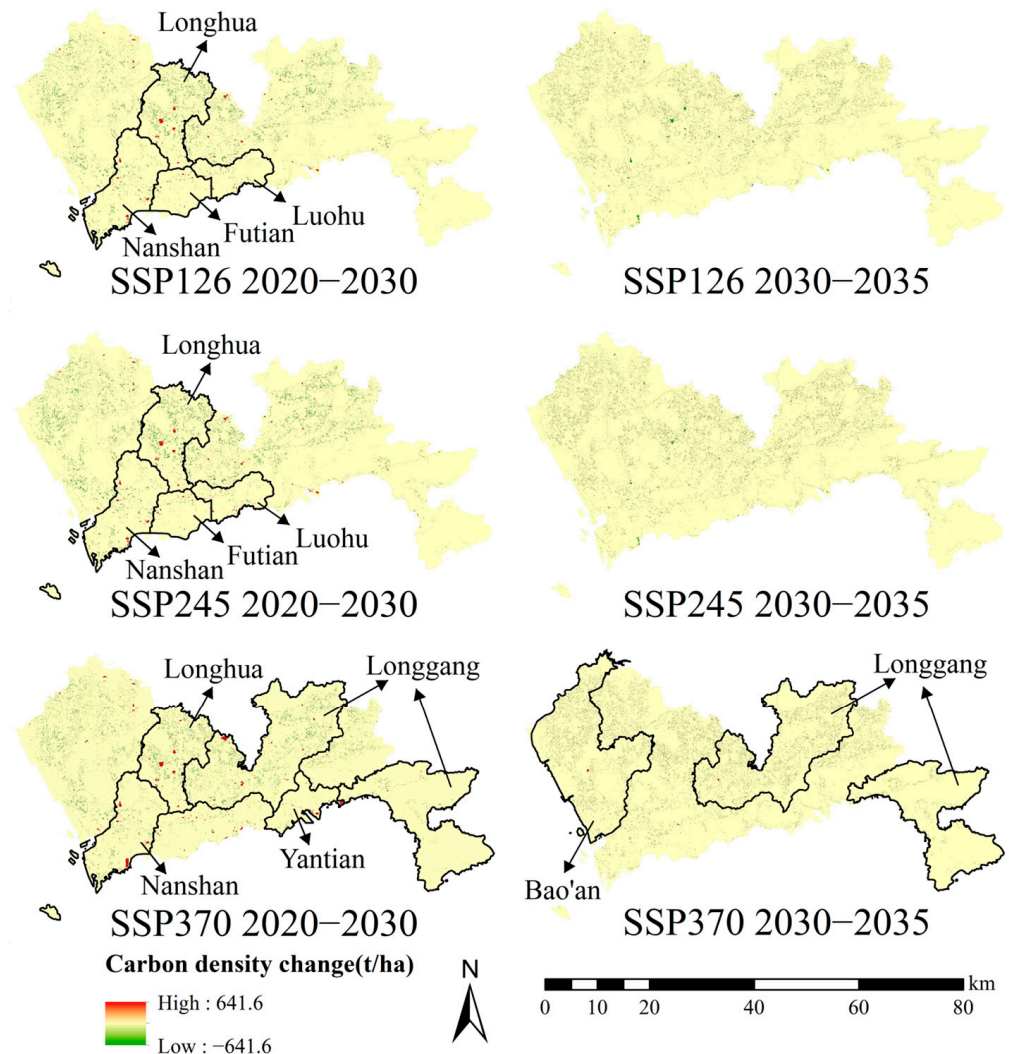


**Figure 7.** Carbon density change for 2020–2030 and 2030–2035 under SSP-RCP scenarios. Note: The left column represents the carbon intensity change from 2020 to 2030 under SSP-RCP scenarios and the right column represents the carbon intensity change from 2030 to 2035 under SSP-RCP scenarios.

#### 4. Conclusions

This study constructed the relationship between land use types and carbon emissions from energy consumption, then integrated it with the SD model and the PLUS model to simulate future land use patterns, carbon emissions, and the variations of carbon density in Shenzhen under multiple SSP-RCP scenarios. Predicted land use patterns vary greatly under different SSP-RCP scenarios. More living land replaces industrial and mining land under scenarios SSP245 than under other scenarios, and these new living lands are mainly located in Bao'an District and Guangming District. Under scenario SSP370, the large amount of population drives other land to convert into living land, which is very rare under scenarios SSP126 and SSP245. Regarding total carbon emissions from 2030 to 2035, there is a decline under scenarios SSP126 and SSP245, so carbon peaking is expected to be achieved under these two scenarios. Under three SSP-RCP scenarios, expansions of areas with high carbon density are mainly located in Nanshan District and Longhua District due

to rapid urban development and high population density. The simulation model applied in this study is advanced and has been validated to be accurate, confirming various trends in land use patterns and carbon emissions under different future scenarios. The results can provide a scientific basis for future urban planning and land expansion in Shenzhen, which is closely related to its carbon emissions and will be conducive to the achievement of carbon peak and carbon neutrality. Shenzhen should pay attention to the environmental impacts when promoting urban development in Nanshan District and Longhua District. In addition, considering the demand for more living land as Shenzhen continues to increase the supply of housing, the rise in carbon density on living land should be curbed as soon as possible through technological progress and the promotion of clean energy [16,71]. In the future, planning factors will be considered in the land use simulation using the PLUS model, machine learning can be adopted in further studies to predict future land use demand more precisely, and the input-output model can be employed to analyze the relationship between land use types and consumption-based carbon emissions rather than production-based carbon emissions.

**Author Contributions:** Conceptualization, W.T. and S.Z.; Data curation, W.T., S.Z. and W.H.; Formal analysis, W.T. and W.H.; Funding acquisition, S.Z.; Investigation, W.H.; Methodology, W.T., L.C. and S.Z.; Supervision, S.Z.; Validation, W.T., L.C. and W.H.; Writing—original draft, W.T. and L.C.; Writing—review & editing, W.T., L.C., S.Z. and W.H. All authors have read and agreed to the published version of the manuscript.

**Funding:** This research was funded by the Open Fund of Key Laboratory of Urban Land Resources Monitoring and Simulation, Ministry of Natural Resources (Grant No. KF-2021-06-068), and the National Natural Science Foundation of China (Grant No. 42007194).

**Data Availability Statement:** The data in the article are detailed in Section 2.1. All the data used are reflected in the article. If you need other relevant data, please contact the authors.

**Acknowledgments:** The authors are thankful to the OpenStreetMap (OSM, <https://www.openstreetmap.org>, accessed on 18 February 2022) for the roads, waterway, waters, and other data in Shenzhen, China. The authors are grateful to WorldPop ([www.worldpop.org](http://www.worldpop.org), accessed on 17 March 2022) for making population data in Shenzhen, China for 2015 available.

**Conflicts of Interest:** The authors declare no conflict of interest.

## Appendix A

**Table A1.** Neighborhood weight of each type of land use.

Land Use Types	Industrial and Mining Land	Traffic Land	Living Land	Agricultural Land and Water Area	Other Land
Neighborhood weight	0.0712	0.2006	0.4469	0.2596	0.0217

**Table A2.** The spatial driving factors of the land use change.

Category	Data	Spatial Resolution	Data Sources
Socioeconomic driving factors	Population	100 m	WorldPop ( <a href="https://hub.worldpop.org/">https://hub.worldpop.org/</a> , accessed on 17 March 2022)
	GDP	1000 m	Resource and Environment Science and Data Center (RESDC) ( <a href="https://www.resdc.cn/">https://www.resdc.cn/</a> , accessed on 16 March 2022)
	The distance from town The distance from highway The distance from railway The distance from other roads	30 m	OpenStreetMap ( <a href="https://www.openstreetmap.org/">https://www.openstreetmap.org/</a> , accessed on 18 February 2022)
	Nighttime light data	1000 m	VIIRS_DNB_VNL V2 ( <a href="https://eogdata.mines.edu">https://eogdata.mines.edu</a> , accessed on 25 February 2022)

Table A2. Cont.

Category	Data	Spatial Resolution	Data Sources
Climatic and environmental driving factors	Annual mean temperature Annual precipitation	500 m	Resource and Environment Science and Data Center (RESDC) ( <a href="https://www.resdc.cn/">https://www.resdc.cn/</a> , accessed on 16 March 2022)
	DEM Slope Degree of relief	30 m	NASADEM_HGT V001 ( <a href="https://www.earthdata.nasa.gov/esds/competitive-programs/measures/nasadem">https://www.earthdata.nasa.gov/esds/competitive-programs/measures/nasadem</a> , accessed on 18 February 2022)
	The distance from waters The distance from waterway	30 m	OpenStreetMap ( <a href="https://www.openstreetmap.org/">https://www.openstreetmap.org/</a> , accessed on 18 February 2022)

## References

- Xu, Q.; Dong, Y.; Yang, R. Urbanization impact on carbon emissions in the Pearl River Delta region: Kuznets curve relationships. *J. Clean. Prod.* **2018**, *180*, 514–523. [\[CrossRef\]](#)
- Arnell, A.; Sitch, S.; Pongratz, J.; Stocker, B.D.; Ciais, P.; Poulter, B.; Bayer, A.D.; Bondeau, A.; Calle, L.; Chini, L.P.; et al. Historical carbon dioxide emissions caused by land-use changes are possibly larger than assumed. *Nat. Geosci.* **2017**, *10*, 79–84. [\[CrossRef\]](#)
- Chu, X.; Huang, X.; Wang, W.; Zhao, R.; Zhang, M.; Wu, C. Land use, total carbon emissions change and low carbon land management in Coastal Jiangsu, China. *J. Clean. Prod.* **2015**, *103*, 77–86. [\[CrossRef\]](#)
- Zhao, R.; Huang, X.; Liu, Y.; Zhong, T.; Ding, M.; Chu, X. Carbon emission of regional land use and its decomposition analysis: Case study of Nanjing City, China. *Chin. Geogr. Sci.* **2015**, *25*, 198–212. [\[CrossRef\]](#)
- Chen, J.; Cui, H.; Xu, Y.; Ge, Q. Long-term temperature and sea-level rise stabilization before and beyond 2100: Estimating the additional climate mitigation contribution from China's recent 2060 carbon neutrality pledge. *Environ. Res. Lett.* **2021**, *16*, 074032. [\[CrossRef\]](#)
- Hu, A. China's Goal of Achieving Carbon Peak by 2030 and Its Main Approaches. *J. Beijing Univ. Technol. Soc. Sci. Ed.* **2021**, *21*, 1–5.
- Zhao, R.; Huang, X. Carbon emission and carbon footprint of different land use types based on energy consumption of Jiangsu Province. *Geogr. Res.* **2010**, *29*, 1639–1649.
- Zhao, R.; Huang, X.; Zhong, T.; Peng, J. Carbon footprint of different industrial spaces based on energy consumption in China. *J. Geogr. Sci.* **2011**, *21*, 285–300. [\[CrossRef\]](#)
- Wu, C.; Li, G.; Yue, W.; Lu, R.; Lu, Z.; You, H. Effects of endogenous factors on regional land-use carbon emissions based on the Grossman decomposition model: A case study of Zhejiang Province, China. *Environ. Manag.* **2015**, *55*, 467–478. [\[CrossRef\]](#)
- Li, M.; Ye, H.; Liao, X.; Ji, J.; Ma, X. How Shenzhen, China pioneered the widespread adoption of electric vehicles in a major city: Implications for global implementation. *WIREs Energy Environ.* **2020**, *9*, e373. [\[CrossRef\]](#)
- Lin, Y.; Zhang, K.; Shen, Z.-J.M.; Miao, L. Charging Network Planning for Electric Bus Cities: A Case Study of Shenzhen, China. *Sustainability* **2019**, *11*, 4713. [\[CrossRef\]](#)
- Mao, F.; Li, Z.; Zhang, K. Carbon dioxide emissions estimation of conventional diesel buses electrification: A well-to-well analysis in Shenzhen, China. *J. Clean. Prod.* **2020**, *277*, 123048. [\[CrossRef\]](#)
- Wang, Q.; Su, M.; Li, R. Toward to economic growth without emission growth: The role of urbanization and industrialization in China and India. *J. Clean. Prod.* **2018**, *205*, 499–511. [\[CrossRef\]](#)
- Zhang, Y.-J.; Liu, Z.; Zhang, H.; Tan, T.-D. The impact of economic growth, industrial structure and urbanization on carbon emission intensity in China. *Nat. Hazards* **2014**, *73*, 579–595. [\[CrossRef\]](#)
- Wang, Z.; Yin, F.; Zhang, Y.; Zhang, X. An empirical research on the influencing factors of regional CO<sub>2</sub> emissions: Evidence from Beijing city, China. *Appl. Energy* **2012**, *100*, 277–284. [\[CrossRef\]](#)
- Ma, X.; Wang, C.; Dong, B.; Gu, G.; Chen, R.; Li, Y.; Zou, H.; Zhang, W.; Li, Q. Carbon emissions from energy consumption in China: Its measurement and driving factors. *Sci. Total Environ.* **2019**, *648*, 1411–1420. [\[CrossRef\]](#)
- Cheng, Z.; Li, L.; Liu, J. Industrial structure, technical progress and carbon intensity in China's provinces. *Renew. Sustain. Energy Rev.* **2018**, *81*, 2935–2946. [\[CrossRef\]](#)
- Stürck, J.; Levers, C.; van der Zanden, E.H.; Schulp, C.J.E.; Verkerk, P.J.; Kuemmerle, T.; Helming, J.; Lotze-Campen, H.; Tabeau, A.; Popp, A.; et al. Simulating and delineating future land change trajectories across Europe. *Reg. Environ. Chang.* **2018**, *18*, 733–749. [\[CrossRef\]](#)
- Jin, G.; Chen, K.; Wang, P.; Guo, B.; Dong, Y.; Yang, J. Trade-offs in land-use competition and sustainable land development in the North China Plain. *Technol. Forecast. Soc. Chang.* **2019**, *141*, 36–46. [\[CrossRef\]](#)
- Wang, Z.; Zeng, J.; Chen, W. Impact of urban expansion on carbon storage under multi-scenario simulations in Wuhan, China. *Environ. Sci. Pollut. Res. Int.* **2022**, *29*, 45507–45526. [\[CrossRef\]](#)
- Schmitz, C.; van Meijl, H.; Kyle, P.; Nelson, G.C.; Fujimori, S.; Gurgel, A.; Havlik, P.; Heyhoe, E.; d'Croz, D.M.; Popp, A.; et al. Land-use change trajectories up to 2050: Insights from a global agro-economic model comparison. *Agric. Econ.* **2014**, *45*, 69–84. [\[CrossRef\]](#)

22. Song, X.-P.; Hansen, M.C.; Stehman, S.V.; Potapov, P.V.; Tyukavina, A.; Vermote, E.F.; Townshend, J.R. Global land change from 1982 to 2016. *Nature* **2018**, *560*, 639–643. [[CrossRef](#)] [[PubMed](#)]
23. O'Neill, B.C.; Kriegler, E.; Riahi, K.; Ebi, K.L.; Hallegatte, S.; Carter, T.R.; Mathur, R.; van Vuuren, D.P. A new scenario framework for climate change research: The concept of shared socioeconomic pathways. *Clim. Chang.* **2014**, *122*, 387–400. [[CrossRef](#)]
24. Tian, J.; Zhang, Z.; Ahmed, Z.; Zhang, L.; Su, B.; Tao, H.; Jiang, T. Projections of precipitation over China based on CMIP6 models. *Stoch. Environ. Res. Risk Assess.* **2021**, *35*, 831–848. [[CrossRef](#)]
25. Duan, R.; Huang, G.; Li, Y.; Zheng, R.; Wang, G.; Xin, B.; Tian, C.; Ren, J. Ensemble Temperature and Precipitation Projection for Multi-Factorial Interactive Effects of GCMs and SSPs: Application to China. *Front. Environ. Sci.* **2021**, *9*, 742326. [[CrossRef](#)]
26. Wei, Y.-M.; Han, R.; Liang, Q.-M.; Yu, B.-Y.; Yao, Y.-F.; Xue, M.-M.; Zhang, K.; Liu, L.-J.; Peng, J.; Yang, P.; et al. An integrated assessment of INDCs under Shared Socioeconomic Pathways: An implementation of C3IAM. *Nat. Hazards* **2018**, *92*, 585–618. [[CrossRef](#)]
27. Chen, Y.; Li, X.; Huang, K.; Luo, M.; Gao, M. High-Resolution Gridded Population Projections for China under the Shared Socioeconomic Pathways. *Earth's Future* **2020**, *8*, e2020EF001491. [[CrossRef](#)]
28. Chen, G.; Li, X.; Liu, X.; Chen, Y.; Liang, X.; Leng, J.; Xu, X.; Liao, W.; Qiu, Y.; Wu, Q.; et al. Global projections of future urban land expansion under shared socioeconomic pathways. *Nat. Commun.* **2020**, *11*, 537. [[CrossRef](#)]
29. Bai, Y.; Deng, X.; Cheng, Y.; Hu, Y.; Zhang, L. Exploring regional land use dynamics under shared socioeconomic pathways: A case study in Inner Mongolia, China. *Technol. Forecast. Soc. Chang.* **2021**, *166*, 120606. [[CrossRef](#)]
30. Zhang, S.; Zhong, Q.; Cheng, D.; Xu, C.; Chang, Y.; Lin, Y.; Li, B. Coupling Coordination Analysis and Prediction of Landscape Ecological Risks and Ecosystem Services in the Min River Basin. *Land* **2022**, *11*, 222. [[CrossRef](#)]
31. Eyring, V.; Bony, S.; Meehl, G.A.; Senior, C.A.; Stevens, B.; Stouffer, R.J.; Taylor, K.E. Overview of the Coupled Model Intercomparison Project Phase 6 (CMIP6) experimental design and organization. *Geosci. Model Dev.* **2016**, *9*, 1937–1958. [[CrossRef](#)]
32. Gidden, M.J.; Riahi, K.; Smith, S.J.; Fujimori, S.; Luderer, G.; Kriegler, E.; van Vuuren, D.P.; van den Berg, M.; Feng, L.; Klein, D.; et al. Global emissions pathways under different socioeconomic scenarios for use in CMIP6: A dataset of harmonized emissions trajectories through the end of the century. *Geosci. Model Dev.* **2019**, *12*, 1443–1475. [[CrossRef](#)]
33. Su, B.; Huang, J.; Mondal, S.K.; Zhai, J.; Wang, Y.; Wen, S.; Gao, M.; Lv, Y.; Jiang, S.; Jiang, T.; et al. Insight from CMIP6 SSP-RCP scenarios for future drought characteristics in China. *Atmos. Res.* **2021**, *250*, 105375. [[CrossRef](#)]
34. Dong, N.; You, L.; Cai, W.; Li, G.; Lin, H. Land use projections in China under global socioeconomic and emission scenarios: Utilizing a scenario-based land-use change assessment framework. *Global Environ. Chang.* **2018**, *50*, 164–177. [[CrossRef](#)]
35. Wang, Z.; Li, X.; Mao, Y.; Li, L.; Wang, X.; Lin, Q. Dynamic simulation of land use change and assessment of carbon storage based on climate change scenarios at the city level: A case study of Bortala, China. *Ecol. Indic.* **2022**, *134*, 108499. [[CrossRef](#)]
36. Zhai, H.; Lv, C.; Liu, W.; Yang, C.; Fan, D.; Wang, Z.; Guan, Q. Understanding Spatio-Temporal Patterns of Land Use/Land Cover Change under Urbanization in Wuhan, China, 2000–2019. *Remote Sens.* **2021**, *13*, 3331. [[CrossRef](#)]
37. Han, J.; Hayashi, Y.; Cao, X.; Imura, H. Application of an integrated system dynamics and cellular automata model for urban growth assessment: A case study of Shanghai, China. *Landsc. Urban Plan.* **2009**, *91*, 133–141. [[CrossRef](#)]
38. Van Dessel, W.; van Rompaey, A.; Szilassi, P. Sensitivity analysis of logistic regression parameterization for land use and land cover probability estimation. *Int. J. Geogr. Inf. Sci.* **2011**, *25*, 489–508. [[CrossRef](#)]
39. Sang, L.; Zhang, C.; Yang, J.; Zhu, D.; Yun, W. Simulation of land use spatial pattern of towns and villages based on CA–Markov model. *Math. Comput. Model.* **2011**, *54*, 938–943. [[CrossRef](#)]
40. Wu, H.; Li, Z.; Clarke, K.C.; Shi, W.; Fang, L.; Lin, A.; Zhou, J. Examining the sensitivity of spatial scale in cellular automata Markov chain simulation of land use change. *Int. J. Geogr. Inf. Sci.* **2019**, *33*, 1040–1061. [[CrossRef](#)]
41. Basse, R.M.; Omrani, H.; Charif, O.; Gerber, P.; Bódis, K. Land use changes modelling using advanced methods: Cellular automata and artificial neural networks. The spatial and explicit representation of land cover dynamics at the cross-border region scale. *Appl. Geogr.* **2014**, *53*, 160–171. [[CrossRef](#)]
42. Li, X.; Chen, G.; Liu, X.; Liang, X.; Wang, S.; Chen, Y.; Pei, F.; Xu, X. A New Global Land-Use and Land-Cover Change Product at a 1-km Resolution for 2010 to 2100 Based on Human–Environment Interactions. *Ann. Am. Assoc. Geogr.* **2017**, *107*, 1040–1059. [[CrossRef](#)]
43. Liang, X.; Guan, Q.; Clarke, K.C.; Liu, S.; Wang, B.; Yao, Y. Understanding the drivers of sustainable land expansion using a patch-generating land use simulation (PLUS) model: A case study in Wuhan, China. *Comput. Environ. Urban Syst.* **2021**, *85*, 101569. [[CrossRef](#)]
44. Li, C.; Yang, M.; Li, Z.; Wang, B. How Will Rwandan Land Use/Land Cover Change under High Population Pressure and Changing Climate? *Appl. Sci.* **2021**, *11*, 5376. [[CrossRef](#)]
45. Shi, M.; Wu, H.; Fan, X.; Jia, H.; Dong, T.; He, P.; Baqa, M.F.; Jiang, P. Trade-Offs and Synergies of Multiple Ecosystem Services for Different Land Use Scenarios in the Yili River Valley, China. *Sustainability* **2021**, *13*, 1577. [[CrossRef](#)]
46. Zhuang, H.; Liu, X.; Yan, Y.; Zhang, D.; He, J.; He, J.; Zhang, X.; Zhang, H.; Li, M. Integrating a deep forest algorithm with vector-based cellular automata for urban land change simulation. *Trans. GIS* **2022**, *26*, 2056–2080. [[CrossRef](#)]
47. Yu, W.; Zhang, Y.; Zhou, W.; Wang, W.; Tang, R. Urban expansion in Shenzhen since 1970s: A retrospect of change from a village to a megacity from the space. *Phys. Chem. Earth Parts A/B/C* **2019**, *110*, 21–30. [[CrossRef](#)]
48. Peng, Y.; Yang, F.; Zhu, L.; Li, R.; Wu, C.; Chen, D. Comparative Analysis of the Factors Influencing Land Use Change for Emerging Industry and Traditional Industry: A Case Study of Shenzhen City, China. *Land* **2021**, *10*, 575. [[CrossRef](#)]

49. Xu, X. China Meteorological Background Dataset. Data Registration and Publishing System of the Resource and Environment Science Data Center of the Chinese Academy of Sciences. 2017. Available online: <https://www.resdc.cn/DOI/doi.aspx?DOIid=39> (accessed on 16 March 2022).
50. Xu, X. China's GDP Spatial Distribution Kilometer Grid Data Set. Data Registration and Publishing System of the Resource and Environment Science Data Center of the Chinese Academy of Sciences 2017. Available online: <https://www.resdc.cn/DOI/doi.aspx?DOIid=33> (accessed on 16 March 2022).
51. Elvidge, C.D.; Zhizhin, M.; Ghosh, T.; Hsu, F.-C.; Taneja, J. Annual Time Series of Global VIIRS Nighttime Lights Derived from Monthly Averages: 2012 to 2019. *Remote Sens.* **2021**, *13*, 922. [[CrossRef](#)]
52. NASA JPL. NASADEM Merged DEM Global 1 Arc Second V001. 2020. Available online: [https://doi.org/10.5067/MEaSURES/NASADEM/NASADEM\\_HGT.001](https://doi.org/10.5067/MEaSURES/NASADEM/NASADEM_HGT.001) (accessed on 5 December 2021).
53. Huang, Y.; Xia, B.; Yang, L. Relationship study on land use spatial distribution structure and energy-related carbon emission intensity in different land use types of Guangdong, China, 1996–2008. *Sci. World J.* **2013**, *2013*, 309680. [[CrossRef](#)]
54. IPCC. *2006 IPCC Guidelines for National Greenhouse Gas Inventories*; Institute for Global Environmental Strategies (IGES): Hayama, Japan, 2006; ISBN 4-88788-032-4.
55. O'Neill, B.C.; Tebaldi, C.; van Vuuren, D.P.; Eyring, V.; Friedlingstein, P.; Hurtt, G.; Knutti, R.; Kriegler, E.; Lamarque, J.-F.; Lowe, J.; et al. The Scenario Model Intercomparison Project (ScenarioMIP) for CMIP6. *Geosci. Model Dev.* **2016**, *9*, 3461–3482. [[CrossRef](#)]
56. Riahi, K.; van Vuuren, D.P.; Kriegler, E.; Edmonds, J.; O'Neill, B.C.; Fujimori, S.; Bauer, N.; Calvin, K.; Dellink, R.; Fricko, O.; et al. The Shared Socioeconomic Pathways and their energy, land use, and greenhouse gas emissions implications: An overview. *Global Environ. Chang.* **2017**, *42*, 153–168. [[CrossRef](#)]
57. Yang, X.; Zhou, B.; Xu, Y.; Han, Z. CMIP6 Evaluation and Projection of Temperature and Precipitation over China. *Adv. Atmos. Sci.* **2021**, *38*, 817–830. [[CrossRef](#)]
58. Shan, Y.; Fang, S.; Cai, B.; Zhou, Y.; Li, D.; Feng, K.; Hubacek, K. Chinese cities exhibit varying degrees of decoupling of economic growth and CO<sub>2</sub> emissions between 2005 and 2015. *One Earth* **2021**, *4*, 124–134. [[CrossRef](#)]
59. Wang, X.; Li, J.; Song, R.; Li, J. 350 cities of China exhibited varying degrees of carbon decoupling and green innovation synergy. *Energy Rep.* **2022**, *8*, 312–323. [[CrossRef](#)]
60. Xu, Q.; Yang, R. The sequential collaborative relationship between economic growth and carbon emissions in the rapid urbanization of the Pearl River Delta. *Environ. Sci. Pollut. Res. Int.* **2019**, *26*, 30130–30144. [[CrossRef](#)]
61. Murakami, D.; Yoshida, T.; Yamagata, Y. Gridded GDP Projections Compatible with the Five SSPs (Shared Socioeconomic Pathways). *Front. Built Environ.* **2021**, *7*, 760306. [[CrossRef](#)]
62. Wu, T.; Lu, Y.; Fang, Y.; Xin, X.; Li, L.; Li, W.; Jie, W.; Zhang, J.; Liu, Y.; Zhang, L.; et al. The Beijing Climate Center Climate System Model (BCC-CSM): The main progress from CMIP5 to CMIP6. *Geosci. Model Dev.* **2019**, *12*, 1573–1600. [[CrossRef](#)]
63. Liu, X.; Liang, X.; Li, X.; Xu, X.; Ou, J.; Chen, Y.; Li, S.; Wang, S.; Pei, F. A future land use simulation model (FLUS) for simulating multiple land use scenarios by coupling human and natural effects. *Landsc. Urban Plan.* **2017**, *168*, 94–116. [[CrossRef](#)]
64. Cohen, J. A Coefficient of Agreement for Nominal Scales. *Educ. Psychol. Meas.* **1960**, *20*, 37–46. [[CrossRef](#)]
65. Ke, Y.; Xia, L.; Huang, Y.; Li, S.; Zhang, Y.; Liang, S.; Yang, Z. The carbon emissions related to the land-use changes from 2000 to 2015 in Shenzhen, China: Implication for exploring low-carbon development in megacities. *J. Environ. Manag.* **2022**, *319*, 115660. [[CrossRef](#)] [[PubMed](#)]
66. Xie, H.; Zhai, Q.; Wang, W.; Yu, J.; Lu, F.; Chen, Q. Does intensive land use promote a reduction in carbon emissions? Evidence from the Chinese industrial sector. *Resour. Conserv. Recycl.* **2018**, *137*, 167–176. [[CrossRef](#)]
67. Li, F.; Li, Z.; Chen, H.; Chen, Z.; Li, M. An agent-based learning-embedded model (ABM-learning) for urban land use planning: A case study of residential land growth simulation in Shenzhen, China. *Land Use Policy* **2020**, *95*, 104620. [[CrossRef](#)]
68. Zeng, Q.; Xie, Y.; Liu, K. Assessment of the patterns of urban land covers and impervious surface areas: A case study of Shenzhen, China. *Phys. Chem. Earth Parts A B C* **2019**, *110*, 1–7. [[CrossRef](#)]
69. Wang, S.; Fang, C.; Wang, Y. Spatiotemporal variations of energy-related CO<sub>2</sub> emissions in China and its influencing factors: An empirical analysis based on provincial panel data. *Renew. Sustain. Energy Rev.* **2016**, *55*, 505–515. [[CrossRef](#)]
70. Li, H.; Mu, H.; Zhang, M.; Gui, S. Analysis of regional difference on impact factors of China's energy—Related CO<sub>2</sub> emissions. *Energy* **2012**, *39*, 319–326. [[CrossRef](#)]
71. Yang, J.; Cai, W.; Ma, M.; Li, L.; Liu, C.; Ma, X.; Li, L.; Chen, X. Driving forces of China's CO<sub>2</sub> emissions from energy consumption based on Kaya-LMDI methods. *Sci. Total Environ.* **2020**, *711*, 134569. [[CrossRef](#)]